Theor. Appl. Climatol. 68, 155–173 (2001)

Theoretical and Applied Climatology

Department of Atmospheric Science, Colorado State University, Fort Collins, Colorado, USA

A climate version of the regional atmospheric modeling system*

G. E. Liston and **R. A. Pielke**

With 12 Figures

Received September 27, 1999
Revised December 11, 1999

Summary

The Regional Atmospheric Modeling System (RAMS) has been widely used to simulate relatively short-term atmospheric processes. To perform full-year to multi-year model integrations, a climate version of RAMS (ClimRAMS) has been developed, and is used to simulate diurnal, seasonal, and annual cycles of atmospheric and hydrologic variables and interactions within the central United States during 1989. The model simulation uses a 200-km grid covering the conterminous United States, and a nested, 50-km grid covering the Great Plains and Rocky Mountain states of Kansas, Nebraska, South Dakota, Wyoming, and Colorado. The model's lateral boundary conditions are forced by six-hourly NCEP reanalysis products. ClimRAMS includes simplified precipitation and radiation sub-models, and representations that describe the seasonal evolution of vegetation-related parameters. In addition, ClimRAMS can use all of the general RAMS capabilities, like its more complex radiation sub-models, and explicit cloud and precipitation microphysics schemes. Thus, together with its nonhydrostatic and fully-interactive telescoping-grid capabilities, ClimRAMS can be applied to a wide variety of problems. Because of non-linear interactions between the land surface and atmosphere, simulating the observed climate requires simulating the observed diurnal, synoptic, and seasonal cycles. While previous regional climate modeling studies have demonstrated their ability to simulate the seasonal cycles through comparison with observed monthly-mean temperature and precipitation data sets, this study demonstrates that a regional climate model can also capture observed diurnal and synoptic variability. Observed values of daily precipitation and maximum and minimum screen-height air temperature are used to demonstrate this ability.

1. Introduction

Current global-scale, general circulation models (GCMs) used to simulate weather and climate do not operate at fine enough grid resolutions to resolve many observed regional weather and climate features. To simulate these meteorological features, regional or limited-area atmospheric models have been used. These models are run at higher resolution than the GCMs and are thus able to better represent mesoscale dynamics and thermodynamics, including processes resulting from finer-scale topographic and land-surface features. Typically the regional atmospheric model is run while receiving lateral boundary-condition inputs from a relatively-coarse resolution atmospheric analysis model or from the output of a GCM. The model simulations performed as part of the Project to Intercompare Regional Climate Simulations (PIRCS) (Takle et al., 1999) are an example of these kinds of simulations. Additional discussions of regional climate modeling efforts can be found in Giorgi (1995), Christensen et al. (1997), McGregor (1997) and Beniston (1998).

Typically, full-year regional climate model integrations have been validated against monthly mean temperature and precipitation observations

* This article has been published for the first time in Theoretical and Applied Climatology 66: 29–47 (2000). Due to the extremely poor quality of the figures caused by the printer we decided to reprint the article again in this issue to guarantee a proper presentation of the paper.
The Publisher

(e.g., Giorgi et al., 1993; Marinucci et al., 1995; Lüthi et al., 1996; Christensen et al., 1997; Christensen et al., 1998). Such studies have been able to demonstrate the model's ability to simulate the seasonal cycles associated with the particular domain of interest. Because of the non-linear interactions between the land surface and atmosphere, a realistic climate model must also be able to simulate the diurnal and synoptic cycles that average to make up the observed monthly climatologies. Mearns et al. (1995), for example, has compared regional climate model outputs with daily observations. As a specific illustrative example of why comparison with daily observations is important, consider an observed monthly precipitation total of 30 mm of water; the behavior of the land-atmosphere system is expected to be quite sensitive to whether this precipitation falls as a one-day, 30 mm precipitation event, or if it falls for 30 days at 1 mm day^{-1}. These differences are expected to influence a wide range of land-surface and atmospheric processes and interactions, including: soil-moisture characteristics, vegetation response, runoff, and surface energy and moisture fluxes. Consequently, efforts to validate the performance of regional climate models should include an assessment of the model's ability to simulate general atmospheric variables at a range of temporal scales. Specifically, a regional climate model should be able to reasonably simulate diurnal, synoptic, and seasonal cycles. An additional measure of a regional climate model's performance, is its competence in simulating interannual variability; something that is not addressed in this paper. The analyses presented herein assesses a regional climate model's performance on diurnal, synoptic, and seasonal time scales.

The Regional Atmospheric Modeling System (RAMS) is a general-purpose, atmospheric-simulation model that includes the equations of motion, heat, moisture, and continuity in a terrain-following coordinate system. This includes a land-surface sub-model that represents the storage and exchange of heat and moisture associated with the atmosphere-terrestrial interface, and cloud, precipitation, and radiation sub-models representing physical processes associated with atmospheric energy and moisture interactions. RAMS has been widely used to simulate relatively short-term (hours to several days) atmospheric and land-surface processes, and the interactions between the two (Pielke et al., 1992; Nicholls et al., 1995). To perform full-year to multi-year regional atmospheric model integrations, a climate version of RAMS (ClimRAMS) has been developed. It contains additional features required to satisfy both computational constraints and time-evolving boundary conditions and land-surface features like vegetation parameters and seasonal snow-cover. The model is used to perform historical simulations where atmospheric analyses data are available to define the lateral boundary-condition forcing. The model could also be configured to use GCM outputs for the lateral boundary conditions. A necessary (although not sufficient) condition for using GCM outputs as lateral boundary conditions, is that realistic regional climate model simulations should result when the analyses lateral boundary conditions are used.

A primary purpose of this ClimRAMS development and validation effort is to provide a version of RAMS that can be used to support vegetation- and snow-related evolution and atmospheric interaction studies. These types of projects require a model capable of simulating the full annual cycle. For example, ClimRAMS has been coupled to the CENTURY ecosystem model (Lu et al., 2001) and the GEMTM ecosystem model (Eastman, 1999). A current deficiency in most regional and global climate model land-surface parameterizations is that they use only simple climatological approaches, based on time-of-year, to define the model vegetation parameters (e.g., leaf area or albedo defined according to Julian date). What is lacking in these schemes is a realistic representation of vegetation response, or changes in live biomass, to atmospheric and hydrologic influences. The climatological approach is incapable of realistically responding to deviations from climatology, such as wetter and drier than average seasons, or to changes in climate. CENTURY (Parton et al., 1996), when coupled with ClimRAMS, provides that biospheric response and allows an analysis of the interactions and feedbacks between the atmosphere and vegetated surface. In addition, ClimRAMS has been used to develop subgrid-scale snow-distribution representations for application in regional and global climate models

(Liston et al., 1999). Both of these research efforts require an atmospheric model capable of performing realistic diurnal, synoptic, and seasonal cycles.

2. Study area and background

For the model simulation discussed herein, the model domain and grid configurations are given in Fig. 1, where a 200-km grid covers the conterminous United States, and a 50-km nested grid covers Kansas, Nebraska, South Dakota, Wyoming, Colorado, and parts of the regions surrounding those states. The fine-grid domain has been chosen to include portions of both the Great Plains and the Rocky Mountains, thus including the different influences of topography and vegetation on atmospheric process found to occur in those regions.

The winter weather over the fine-grid area of Fig. 1 is dominated by frequent migratory high and low pressure systems that are associated with the polar jet stream and its associated polar front. If the jet stream flow is basically zonal, the air masses associated with the front are Pacific in origin, producing substantial snows in the mountains, and relatively mild air just to the lee of these barriers. Further east, the weather in the Great Plains is cooler, with some air from Canada entrained south into the region west of the low pressure systems. Occasionally, Arctic high pressure systems travel southward over the region producing the area's coldest weather of the year. These intrusions of Arctic air occur when the polar jet stream travels far north into Alaska and northwest Canada, before plunging south over the Great Plains. Upslope snows frequently occur in the western High Plains during these cold outbreaks.

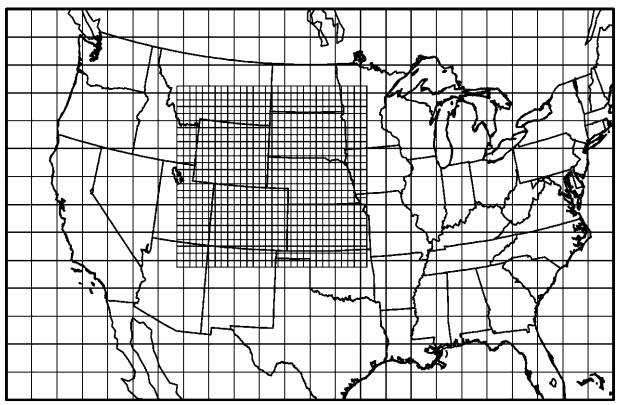

Fig. 1. ClimRAMS simulation domain and grid configuration. The coarse and fine grid intervals are 200 km and 50 km, respectively

Spring is a transition season when the higher sun angles can produce warmer days, yet cold air masses still occasionally travel southward bringing heavy snows to the Plains. In the western high Plains, March and April are the snowiest months of the year. At this time in the eastern high Plains, thunderstorms become common. Thunderstorms can often be quite intense at this time of the year as a result of strong solar surface insolation and relatively cold air aloft. The tornado season in that region peaks in April, May, and June, as a still vigorous polar jet stream provides large changes in wind speed and direction with altitude. This large wind shear provides the initial horizontal wind circulation for tornadic thunderstorms, when the wind shear is tilted on its side by intense thunderstorm updrafts and downdrafts. A tornado can subsequently be produced when this horizontal wind circulation is concentrated into a small area by intense updrafts. By summer, the polar jet has typically migrated far to the north. Rainfall becomes dominated by topographically-heated upslope flows, and weak migratory low pressure systems. During this period, the weather-pattern changes are relatively slow. Organized clusters of thunderstorms, called mesoscale convective systems (MCSs), can develop and are associated with weak frontal boundaries or higher terrain. These MCSs usually move eastward in response to the weak westerly winds in the middle and upper troposphere found during this time of the year. A dryline boundary usually forms in the western Plains, separating humid air coming from the Gulf of Mexico from dry air originating in the desert Southwest and northern Mexico. During summer, thunderstorms frequently form in this dryline region.

In late summer, the Mexican monsoon starts to affect the western portion of the region. Substantial rains often occur as moisture originating in tropical Pacific Ocean is advected northward into the southern Plains and southern Rocky Mountains. This monsoon flow regime weakens in late August, and relatively dry weather, dominated by persistent and often nearly stationary high pressure systems, begins to dom-

inate the fall months. Occasionally, snowstorms occur as early as September in the northern and central Great Plains and Rocky Mountains, when the polar jet stream migrates southward in early fall.

In general, the climate of the Great Plains and Rocky Mountains of the United States displays a strong seasonal cycle. Each season is characterized by significantly different meteorological conditions that are described by weather events such as the passage of frontal systems and the production of convective storms. These weather events operate on time scales ranging from several hours to a few days. ClimRAMS has been designed to represent these individual weather events and their seasonal evolution.

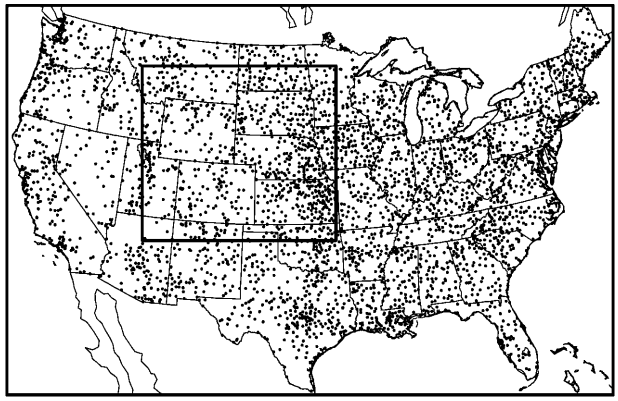

Fig. 2. Locations of National Climatic Data Center (NCDC) Summary-of-the-Day (SOD) meteorological stations. The inset box defines the fine-grid boundary shown in Fig. 1

Model validation is performed using National Climatic Data Center (NCDC) Summary-of-the-Day (SOD) meteorological-station precipitation and maximum and minimum air temperature data. These SOD observations are available throughout the year and have a daily temporal coverage that includes approximately 3800 stations distributed across the United States (Fig. 2). Also shown in Fig. 2 is the outer-boundary of the 50-km grid from Fig. 1. The SOD station data are gridded to the 50-km ClimRAMS grid using an objective analysis scheme (Cressman, 1959), and then compared with the model outputs. Before this comparison is made, the model-produced maximum and minimum temperature fields are adjusted to account for the difference between the model and station elevations. This is done by gridding the station elevations to the model grid, and then applying a spatially- and temporally-constant lapse rate of $-6.5\,^{\circ}\mathrm{C\,km^{-1}}$ to the difference between the station and model topography. The resulting temperature correction (Fig. 3) is then added to the model temperatures. We have chosen to adjust the model temperatures

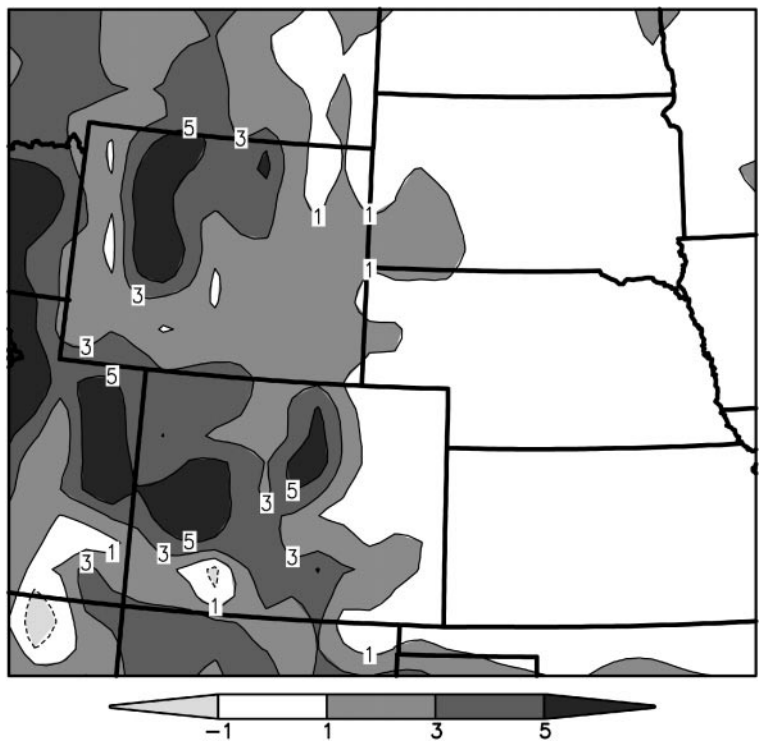

Fig. 3. Temperature correction (°C) added to the model temperatures to account for differences between station and model elevations; in the western area of the fine-grid domain the model topography is generally higher than the station elevations

to the station elevations to avoid any modification of the observed data. We also recognize that the observations are biased towards lower elevations, and that, in some sense, the modeled temperatures may be more representative of the true grid-cell averages. The observational data sets are known to include other errors, such as urban heat island effects on temperature (Karl et al., 1988; Gallo et al., 1996) and wind and wetting effects on precipitation (Groisman and Legates, l994), that have not been taken into account in our model validation.

Copeland et al. (1996) used a preliminary version of ClimRAMS to perform two month-long simulations for July 1989. These simulations were used to compare the influence of changing the vegetation distribution over the United States from its pre-settlement, natural vegetation distribution (from, say, 200 years ago), to the current vegetation distribution. To be compatible with the Copeland et al. (1996) model simulations, 1989 was chosen for the model simulations presented herein. To highlight how representative 1989 is of the area's general climatology, 15 years spanning the period 1982 through 1996, of monthly mean, daily precipitation and screen-height average maximum and minimum air temperature observations were gridded to the 50-km grid in Fig. 1 and averaged over the domain represented by that grid. These monthly data were used to compute yearly averages. Over the 15-year period the mean temperature was 8.52 °C, with a standard deviation of 0.65 °C, and a 1989 mean of 8.29 °C. The mean precipitation over the period was 1.37 mm day^{-1}, with a standard deviation of 0.16 mm day^{-1}, and a 1989 mean of 1.13 mm day^{-1}.

In what follows, a summary of the main ClimRAMS components, initial and boundary conditions, and general model configuration are presented. Detailed comparisons of the model results and the observational data sets are presented in Section 4. Section 5 summarizes our general findings and conclusions.

3. Model description

3.1 ClimRAMS

RAMS was developed at Colorado State University primarily to facilitate research into mesoscale and regional, cloud and land-surface atmospheric phenomena and interactions (Pielke, 1974; Tripoli and Cotton, 1982; Tremback et al., 1985; Pielke et al., 1992; Walko et al., 1995a). The model is fully three-dimensional and non-hydrostatic (Tripoli and Cotton, 1980). The RAMS horizontal grid uses an oblique (or rotated) polar-stereographic projection, where the pole of the projection is rotated to an area near the center of the simulation domain, thus minimizing the projection distortion in the main area of interest. The grid's vertical structure uses a σ_z terrain-following coordinate system (Gal-Chen and Somerville, 1975; Clark, 1977; Tripoli and Cotton, 1982), where the top of the model is flat and the bottom follows the terrain. An Arakawa-C grid configuration is used in the model, where the velocity components u, v, and w are defined at locations staggered one-half a grid length in the x, y, and z directions, respectively, from the thermodynamic, moisture, and pressure variables (Arakawa and Lamb, 1977). Grid nesting is available to provide high spatial resolution in selected areas, while covering a larger domain at lower resolution. The grid-nesting technique follows Clark and Farley (1984) and Clark and Hall (1991), with a generalization for stretched grids and a spatially-variable nesting ratio described by Walko et al. (1995b). This implementation includes a two-way communication of all prognostic variables between any nested grid and its parent grid, and the methodology conserves mass, momentum, and internal thermodynamic energy.

ClimRAMS contains all of the above features, with the addition of several changes designed to allow full-year to multi-year integrations. To meet the requirements of a regional model running at both weather and climate time scales, several modifications to the base modeling system were made, including: (1) sea-surface temperatures and vegetation parameters are updated daily; (2) a collection of routines that simulate grid-scale snow accumulation, snow melt, and their effects on surface hydrology and surface energy exchanges were added; (3) a moisture- and precipitation-physics scheme for long model runs was implemented; and (4) simplified incoming shortwave and longwave radiation schemes were introduced. Details of the ClimRAMS model implementation and physics

representations are provided in the following paragraphs.

In ClimRAMS, the Mahrer and Pielke (1977) shortwave and longwave radiation model is used in conjunction with the scheme presented by Thompson (1993) to account for the presence of clouds. In this scheme a threshold relative humidity is used to define the presence of clouds, and Neiburger's (1949) curve is used to relate cloud depth to cloud albedo for shortwave radiation. For longwave radiation, these defined clouds modify the downward radiative fluxes following Hurley and Boers (1996). Other, more complex, shortwave and longwave radiation schemes are also available in ClimRAMS/RAMS (Chen and Cotton, 1983, 1987; Harrington, 1997).

In addition to the standard explicit cloud and precipitation microphysics representation generally available in RAMS (Meyers et al., 1992; Meyers, 1995; Walko et al., 1995a), two additional precipitation schemes have been implemented in ClimRAMS. The most simple precipitation scheme is based on the ''dump-bucket'' parameterization used in the RAMS forecast model (Cotton et al., 1995). In this parameterization, water vapor in excess of saturation is assumed to condensate, and then the precipitation amount is computed and removed from the saturated layer by applying a precipitation efficiency that is a function of the saturated-layer temperature (Rhea, 1978). The resulting precipitation is assumed to reach the ground without any further interactions with the atmosphere. This method does not distinguish between the various types of precipitation (e.g., rain, snow, hail), and thus additional information is required to identify whether liquid (rain) or ice-phase (snow) precipitation reaches the ground. This is accomplished by assuming that when the air temperature in the lowest atmospheric model layer is less than 2.0 °C, snow reaches the ground; all other conditions lead to rain (Auer, 1974). The explicit cloud physics parameterization of Schultz (1995) has also been implemented in ClimRAMS. The complexity of this precipitation scheme lies between the full microphysics and the ''dump-bucket'' options. Schultz (1995) includes five categories of condensate in this precipitation sub-model: cloud liquid, assumed to have a zero fall velocity; pristine cloud-ice crystals; rain; snow; and precipitating ice (includes graupel, sleet, and hail). Condensation, evaporation, collection, freezing, and melting are all accounted for as part of the precipitation evolution and interactions with the surrounding atmosphere. Both the ''dump-bucket'' and Schultz schemes reduce the computational requirements considerably over the full microphysics option, with apparently only minimal loss in precipitation skill score for the 50-km grid increment considered in this study. For the case of the ''dump-bucket'' scheme, the ClimRAMS computation time is approximately reduced by half when compared to the full microphysics scheme. In addition to simulating large-scale precipitation, ClimRAMS uses a modification of the generalized form (Molinari, 1985) of the Kuo (1974) convective parameterization (Tremback, 1990) to account for convection-produced precipitation.

Each surface grid cell in RAMS is divided into three different surface-type classes: water, bare soil, and vegetated. Prognostic temperature and moisture variables are carried for the bare soil and vegetated surfaces. A vegetated surface is assumed to have bare ground under the vegetation canopy. For bare soil, the McCumber and Pielke (1981) and Tremback and Kessler (1985) multi-level prognostic soil model is used. The surface temperature is determined from the surface energy balance, accounting for incoming and outgoing shortwave and longwave radiation, latent and sensible heat flux, and the soil conductive flux. The soil model includes equations for the diffusion of heat and moisture following Philip and DeVries (1957) and Clapp and Hornberger (1978). The soil thermal properties are temporally-evolving as a function of soil moisture. The soil-moisture boundary condition at the deepest soil level is held constant in time and equal to the initial value. Plant transpiration extracts soil moisture through the roots by the method outlined in Avissar and Mahrer (1982). The vertical root profile is defined to be the same as that used in the Biosphere-Atmosphere Transfer Scheme (BATS) (Dickinson et al., 1986). The vegetation classification and parameter descriptions also follow those used in BATS, where there are 18 vegetation classifications. Also following BATS, the surface characteristics of albedo, emissivity, roughness

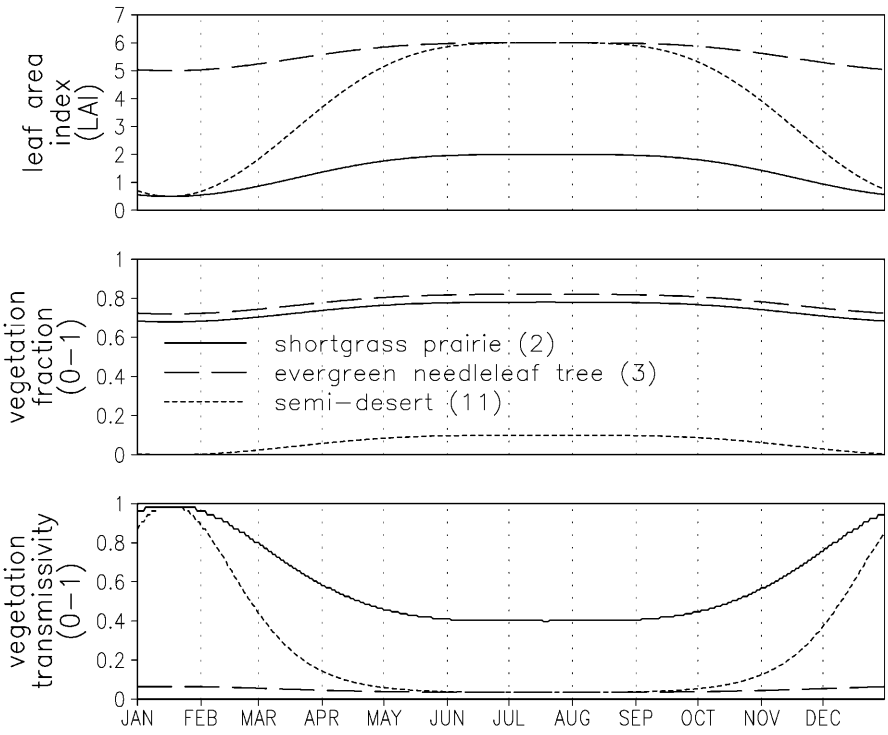

Fig. 4. Example seasonal evolutions of leaf area index, vegetation fraction, and canopy transmissivity to solar radiation, for shortgrass prairie, evergreen needleleaf tree, and semi-desert vegetation classifications. The fine-grid spatial distribution of these classes are given in Fig. 7

length, displacement height, canopy transmissivity to solar radiation, fractional vegetation coverage, and leaf area index (LAI) are defined based on climatological temperatures and vegetation type. The seasonal variation of vegetation canopy transmissivity, fractional coverage, and LAI are predefined by assigning a cosine function to the climatological temperatures used to compute these parameters. Example seasonal evolutions of these parameters are provided in Fig. 4. The soil-texture-class spatial distribution is defined according to the United States Department of Agriculture, STATSGO soils database (Miller and White, 1998). The soil-texture distribution for the fine grid in Fig. 1 is given in Fig. 5. The temperature of the bottom soil layer varies following the deep-soil temperature model of Deardorff (1978). The model implementation presented herein uses 10 soil layers, with the bottom of each layer at the following levels (m): 0.05, 0.125, 0.2, 0.3, 0.45, 0.65, 0.95, 1.3, 1.65 and 2.0.

The surface-layer fluxes of heat, momentum, and water vapor are computed using the method of Louis (1979, 1982), who fitted analytic curves to the flux-profile relationships determined by Businger et al. (1971). This scheme is applied to each grid-cell fraction of water, bare-soil, and vegetated surfaces, and the resulting fluxes are weighted according to the fractional area of each surface type. The surface roughness is specified over land according to vegetation type, and over water it is a function of wind speed. Parameterization of the horizontal and vertical diffusion coefficients is done using K-theory based on Smagorinski (1963), where the mixing coefficients are related to the fluid deformation rate, and corrections are made to account for the influence of Brunt-Väisälä frequency (Hill, 1974) and Richardson number (Lilly, 1962).

In ClimRAMS, a simple snow sub-model accounts for key features of the snowcover and its atmospheric and hydrologic interactions and feedbacks. The primary components of the snow model are: (1) precipitation is assumed to fall as snow if the temperature of the lowest atmospheric model level is $< 2.0\,^{\circ}\mathrm{C}$ (Auer, 1974); (2) the snowpack is represented by one layer of constant density and thermal properties; (3) the albedo decreases linearly with snow depth, towards the vegetation albedo, when the snow-water-equivalent depth is less than 5 cm, and is modified depending on whether the snow is dry (albedo $= 0.8$) or melting (albedo $= 0.5$) (Male and Gray, 1981); (4) the ground heat-flux computation is modified as a function of snow depth; (5) the surface roughness is modified when snow is present; (6) the snow surface

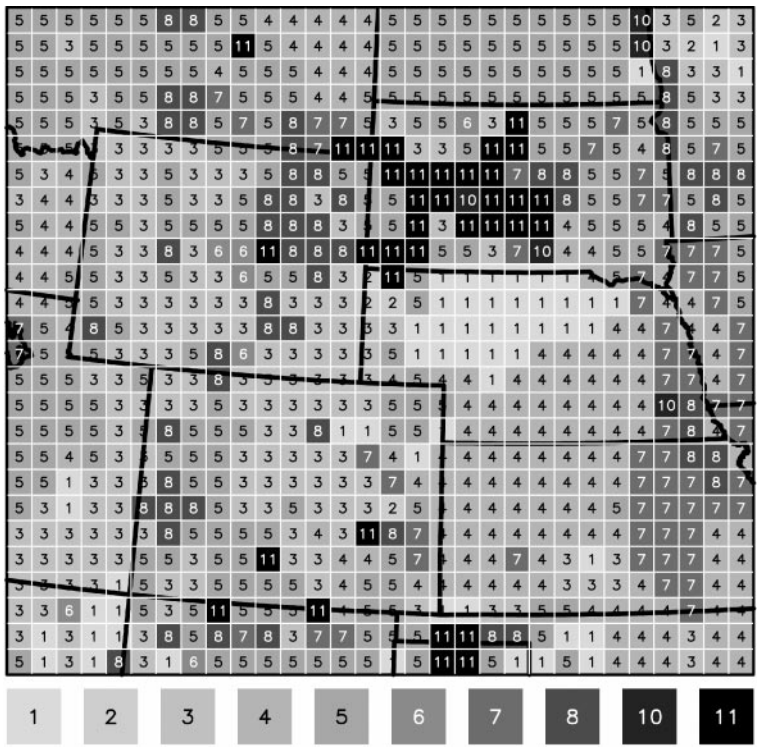

Fig. 5. The soil-texture-class spatial distribution for the fine grid in Fig. 1, defined according to the United States Department of Agriculture, STATSGO soils database (Miller and White, 1998). The numbers correspond to the following ClimRAMS soil classes: 1, sand; 2, loamy sand; 3, sandy loam; 4, silt loam; 5, loam; 6, sandy clay loam; 7, silty clay loam; 8, clay loam; 10, silty clay; 11, clay. Soil class 9 (sandy peat) and 12 (peat) are not included in this domain at this resolution

temperature is constrained to be $\leq 0\,^{\circ}\mathrm{C}$; (7) the available energy to melt snow is computed as part of the surface energy balance; and (8) snow meltwater is added to the soil-moisture store. Additional details of the ClimRAMS snow submodel, and the model's ability to simulate observed snow distributions, can be found in Liston et al. (1999).

3.2 Boundary and initial conditions

The model topography is defined using a global, 30 arc-second latitude-longitude (approximately 1-km) topographic data set called GTOPO30 (Gesch et al., 1999) and available through the United States Geological Survey's (USGS) Earth Resources Observation Systems (EROS) Data Center. In processing these data for the ClimRAMS grids, each coarse grid cell is assigned an elevation equal to the mean of the coincident collection of fine grid cells, thus ensuring compatibility of terrain heights between nested model grids, while still allowing higher-resolution terrain features to be included in the finer grids. The topographic distribution for the fine grid in Fig. 1 is given in Fig. 6. The model vegetation distribution is defined using the International Geosphere-Biosphere Programme (IGBP) land-cover classification, available through the USGS EROS Data Center. The dominant land-cover class coincident with each ClimRAMS grid cell is used to define the model's land-cover distribution. The vegetation distribution for the fine grid in Fig. 1 is given in Fig. 7. The water-surface temperatures are defined according to National Oceanic and Atmospheric Administration (NOAA) sea-surface-temperature analyses produced weekly on a global one-degree grid (Reynolds and Smith, 1994), and interpolated to the ClimRAMS grids.

The method used to generate snow-water-equivalent distribution initial conditions closely follows Liston et al. (1999), and are provided by first generating observed snow-water-equivalent depth distributions for the conterminous United States. This is done by merging two data sets: the National Operational Hydrologic Remote Sensing Center (NOHRSC) snow-water-equivalent depth data, and the NCDC SOD meteorological-station snow-depth data. The NOHRSC data cover the western United Sates on a 30 arc-second latitude-longitude grid, and are derived from a variety of remote sensing and ground-based observations (Carroll, 1997). They are

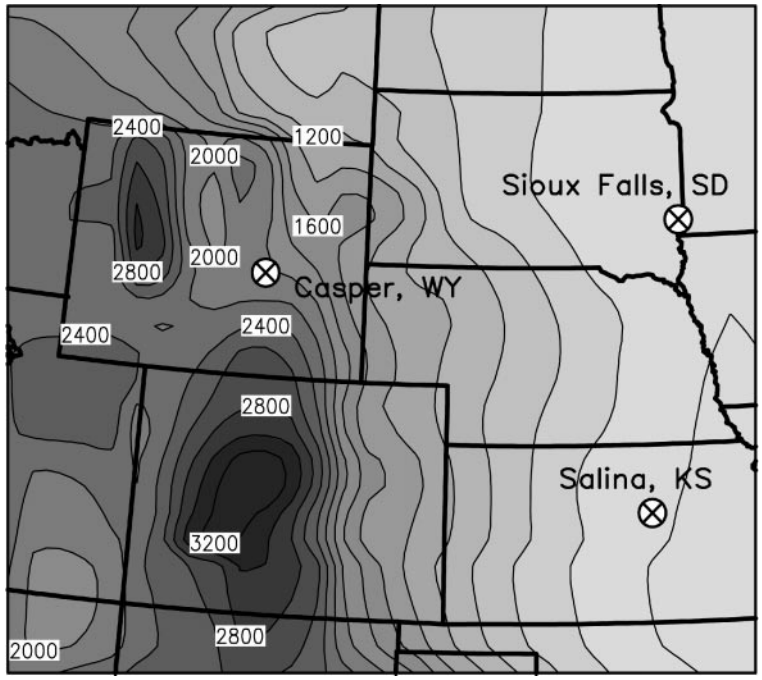

Fig. 6. The topographic distribution for the fine grid in Fig. 1. Also shown are the city/grid locations used in Figs. 11 and 12

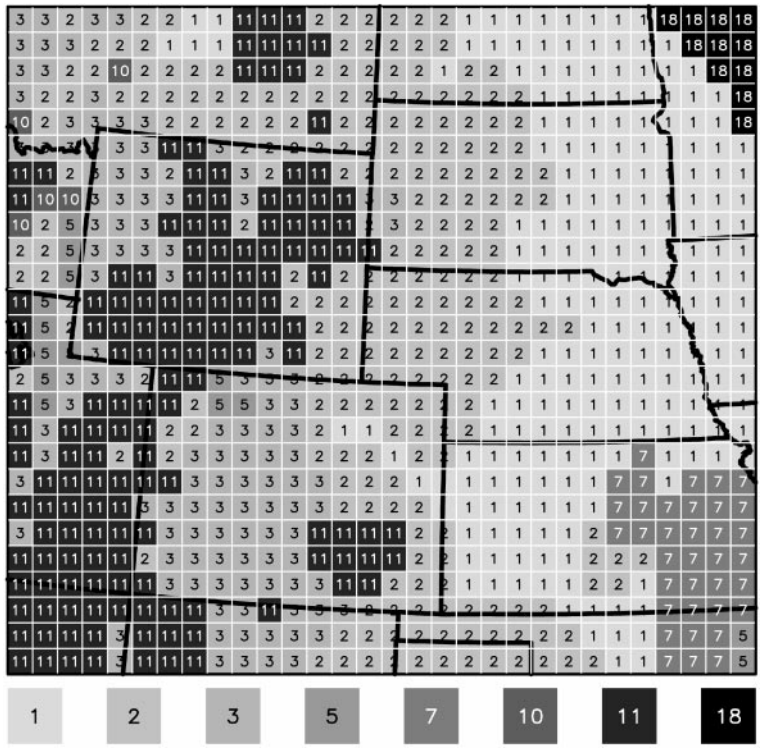

Fig. 7. The vegetation distribution for the fine grid in Fig. 1, defined according to the International Geosphere-Biosphere Programme (IGBP) land-cover classification. The numbers correspond to the following ClimRAMS vegetation classes: 1, crop/mixed farming; 2, short-grass prairie; 3, evergreen needleleaf tree; 5, deciduous broadleaf tree; 7, tallgrass prairie; 10, irrigated crop; 11, semi-desert; 18, mixed woodland. Vegetation class 4 (deciduous needleleaf tree), 6 (evergreen broadleaf tree), 8 (desert), 9 (tundra), 12 (ice cap/glacier), 13 (bog/marsh), 14 (inland water), 15 (ocean), 16 (evergreen shrubland), and 17 (deciduous shrubland) are not included in this domain at this resolution

available approximately twice per week during the middle-winter through early-summer months. The SOD snow-depth observations are available throughout the year and have a daily temporal coverage that includes the stations given in Fig. 2. The SOD station data are first gridded to a 5-km grid using an objective analysis scheme (Cressman, 1959). The resulting snow-depth distributions are then converted to snow-water-equivalent distributions using the snow-

Table 1. Snow densities used to convert snow depth to snow-water-equivalent depth using to the snow-classification distribution of Sturm et al. (1995)

Snow Classification	Snow Density ($kg\,m^{-3}$)
Tundra	280
Taiga	225
Alpine	250
Prairie	250
Maritime	300
Ephemeral	350

classification distribution of Sturm et al. (1995), where the snow density used for each of the snow classes is given in Table 1. The NOHRSC data are then gridded to the 5-km grid used for the SOD data, and the two data sets are merged to provide spatially continuous, 5-km coverage over the conterminous United States. Because of the broader collection of data sources used in the NOHRSC data sets (including mountain-based United States Natural Resources Conservation Service SNOTEL (SNOw TELemetry) observations), the NOHRSC data are used wherever both data sets are coincident. These 5-km data are then regridded to the 200 and 50-km RAMS grids (Fig. 1) for use in the model simulations. As part of the model simulations, any required conversion from snow depth to snow-water-equivalent depth, and back, is accomplished using the Sturm et al. (1995) snow-classification distribution and the density values provided in Table 1.

Horizontal wind components, relative humidity, air temperature, and geopotential height are required to be used as atmospheric lateral boundary conditions for the ClimRAMS simulations. These data sets are available from the National Centers for Environmental Prediction (NCEP) in the form of six-hourly atmospheric reanalyses products, on pressure levels and a global 2.5° latitude by 2.5° longitude grid (Kalnay et al., 1996). The variables are interpolated to the ClimRAMS coarsest grid, and then linearly interpolated in time to each model time step. Lateral boundary-condition nudging is performed on the two outer-boundary grid cells of the 200-km grid following the flow-relaxation scheme of Davies (1976, 1983); there is no nudging performed in the interior of the coarse grid or over any of the fine grid. Initial atmospheric fields are also provided by the NCEP reanalyses.

Soil moisture initial distributions are generated by first defining a spatially-constant soil moisture content over the domain, and running the model for one year. The soil moisture distribution on the last day of that simulation is then used as the initial conditions for the next year's simulation. A spatially-constant soil moisture of 55% of the total water capacity was used to start the one-year soil-moisture ''spin-up'' simulation. The simulation started on 1 January, and the 31 December soil moisture distribution was used as the 1 January soil moisture initial conditions for the simulations presented herein.

For the model simulations discussed in this paper, ClimRAMS has been set up with the horizontal grid configuration summarized in Fig. 1, and with 20 vertical levels having a thickness of 119 meters at the surface and stretching to 2000 meters at the 23-km domain top. The simulations span the period 1 January through 31 December 1989. The model uses a 120-second time step for both the 200 and 50-km grids. The pole point for the oblique polar-stereographic projection is defined to be 40° N latitude and 100° W longitude. The land-surface sub-model is called at every atmospheric-dynamics time step, and the simple ''dump-bucket'' large-scale precipitation scheme is used. Under the assumption that the convective and radiative tendencies evolve on a time scale greater than that defined by the model dynamics time step, the convective parameterization and radiation schemes are called every 7.5 and 30 minutes, respectively.

4. Results

The model's ability to simulate domain-averaged daily maximum and minimum screen-height air temperature and daily precipitation are shown in Fig. 8, where these variables have been averaged over the 50-km grid given in Fig. 1. The observations and model results are shown, and the difference between these two values (model minus observed) are plotted. The difference plots include the 30-day running mean of the daily values. Also shown are the mean (mn) and standard deviation (sd) for each panel and

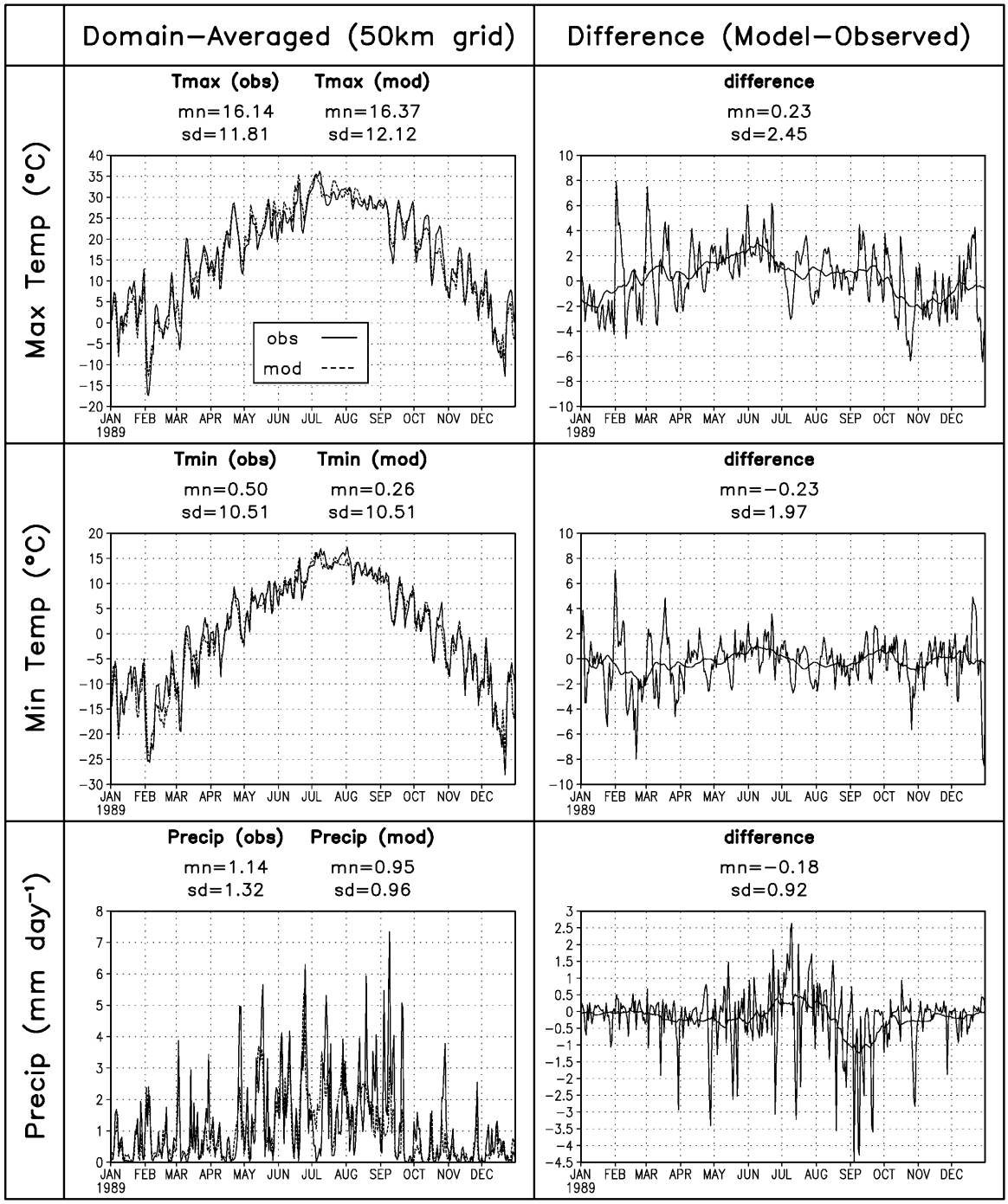

Fig. 8. Modeled and observed, domain-averaged daily maximum and minimum screen-height air temperature and daily precipitation, where these variables have been averaged over the 50-km grid given in Fig. 1. Also shown is the difference between the model and observations, and the 30-day running mean of the difference values. Included are the mean (mn) and standard deviation (sd) for each panel and variable

variable plotted in the figure. The model is found to reproduce the annual cycle of these primary climate variables and it also closely reproduces the synoptic cycle that varies on an approximately one-week time scale. Over the year, the model-simulated daily maximum and minimum screen-height air temperatures average 0.23 °C high and 0.23 °C low, respectively. The deviation from observed values can vary approximately ± 3 °C on any given day, but deviations outside

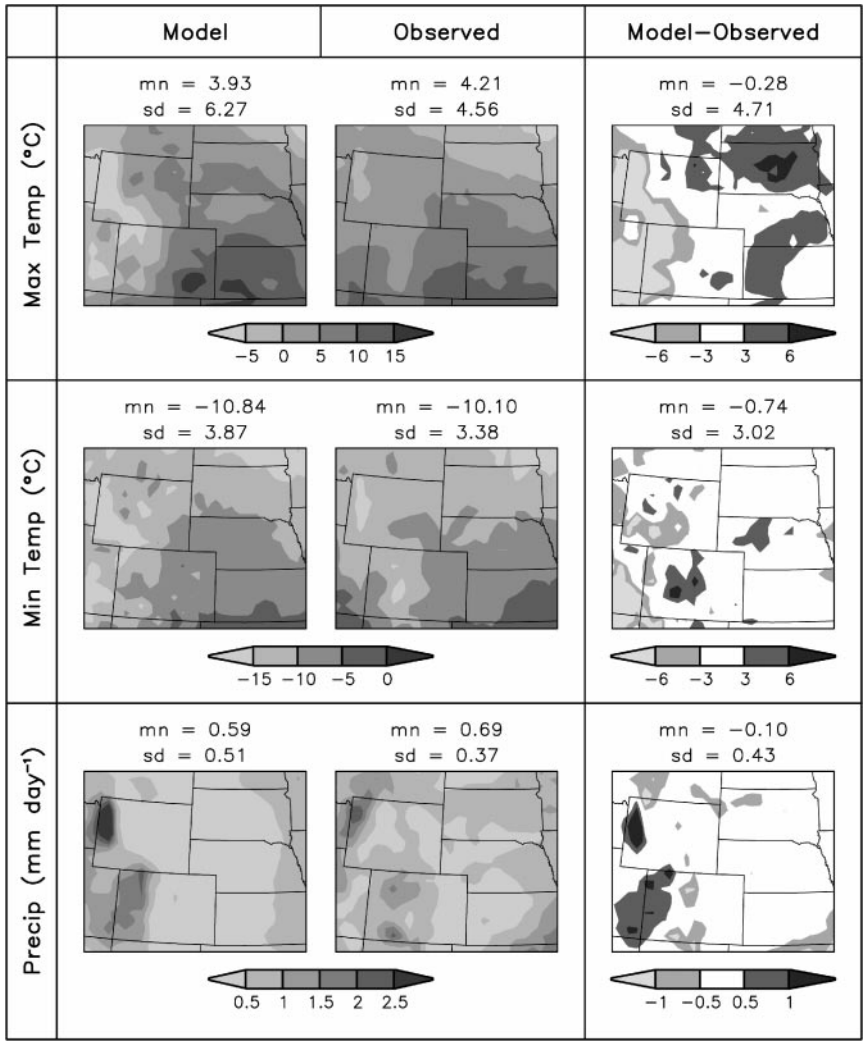

Fig. 9. The winter spatial patterns of maximum and minimum daily screen-height temperature and daily precipitation, averaged over January through March. Shown are the modeled and observed fields, and the differences between the two. Also included are the mean (mn) and standard deviation (sd) for each panel and variable

this range are rare. Over the year, the model-simulated daily precipitation averages 0.18 mm day^{-1} too low. The model captures the timing of individual precipitation events throughout the year, and the magnitudes are well-simulated during the fall and winter months. During spring and summer, the model produces both excess and inadequate precipitation amounts, with the greatest underestimates occurring during May–June and August–September. The individual daily precipitation peaks are rarely captured by the model.

The winter (January through March averages) spatial patterns of maximum and minimum daily screen-height temperature and daily precipitation are given in Fig. 9. Shown are the modeled and observed fields, and the differences between them (model minus observed). The model is found to generally capture the observed spatial patterns, and produces spatially-averaged maximum and minimum temperatures 0.28 °C and 0.74 °C less than those observed, respectively, and spatially-averaged precipitation of 0.10 mm day^{-1} less than that observed. The modeled maximum temperature is too low by as much as 7 °C in portions of the western (mountainous) region of the domain, and too high by as much as 6 °C in portions of the eastern (prairie) region of the domain. The precipitation produced over the Teton mountain range in north-western Wyoming is greater than that observed.

The summer (June through August averages) spatial patterns of maximum and minimum daily temperature and daily precipitation are given in Fig. 10. Shown are the modeled and observed fields, and the differences between them (model

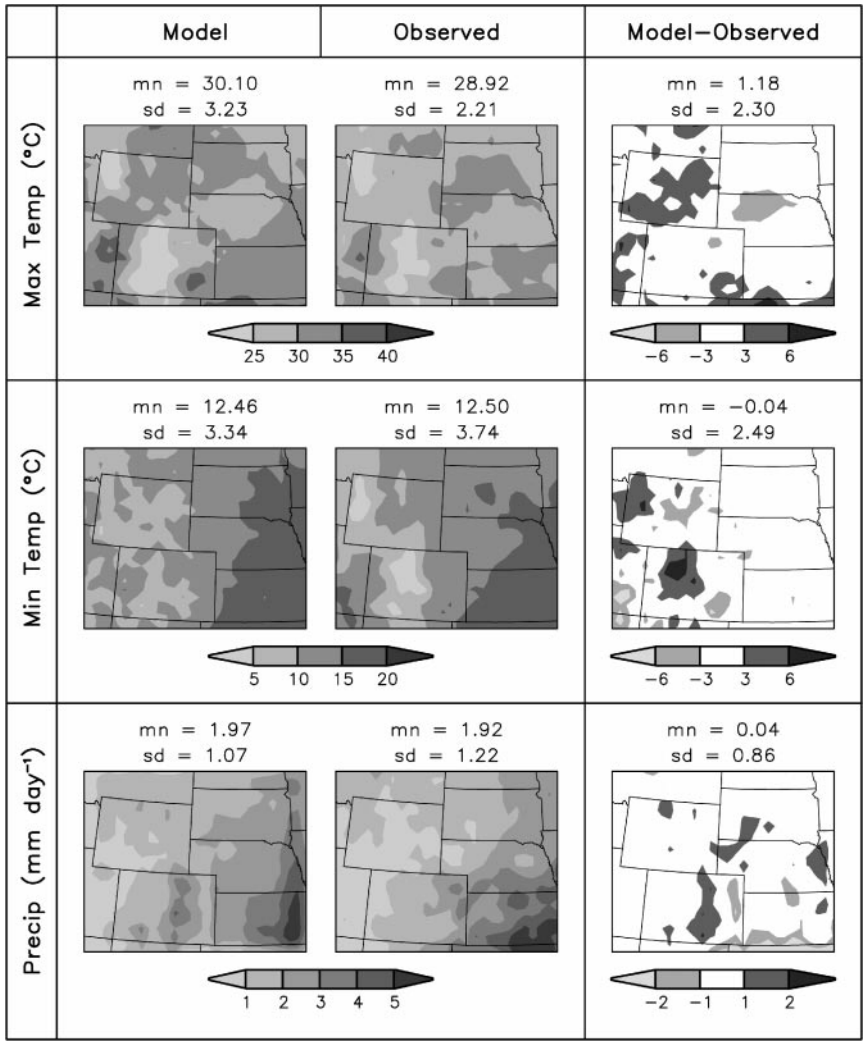

Fig. 10. Same as Fig. 9, but for summer, averaged over June through August

minus observed). The model is found to generally capture the observed spatial patterns, and produces spatially-averaged maximum and minimum temperatures 1.18 °C greater and 0.04 °C less than those observed, respectively, and spatially-averaged precipitation of 0.04 mm day^{-1} more than that observed. The maximum-temperature winter cold bias present in the western part of the domain is not present in the summer period. The observed precipitation maximum in the south-east corner of the domain is simulated by the model, although there is some suggestion that the model's coarse- and fine-grid information transfer influences the precipitation produced in this area, and that the convective parameterization has been unable to correctly represent the transition from the fine to coarse grid at the fine-grid outflow boundary. The temperature fields do not display any similar misrepresentation.

The annual cycle of daily maximum and minimum screen-height air temperature, at the model grid cells corresponding to three cities within the fine-grid domain, is given in Fig. 11. These cities are identified by the markers in Fig. 6, and are: Salina, Kansas; Sioux Falls, South Dakota; and Casper, Wyoming. They each exist in different temperature and precipitation regimes, and the model has been able to capture this variability. Differences between the model and observations are also plotted in Fig. 11, where a 7-day running mean has been applied to the data to improve clarity. The synoptic cycles are captured very well in both the maximum and minimum temperatures, although magnitudes of the modeled values can differ by several degrees

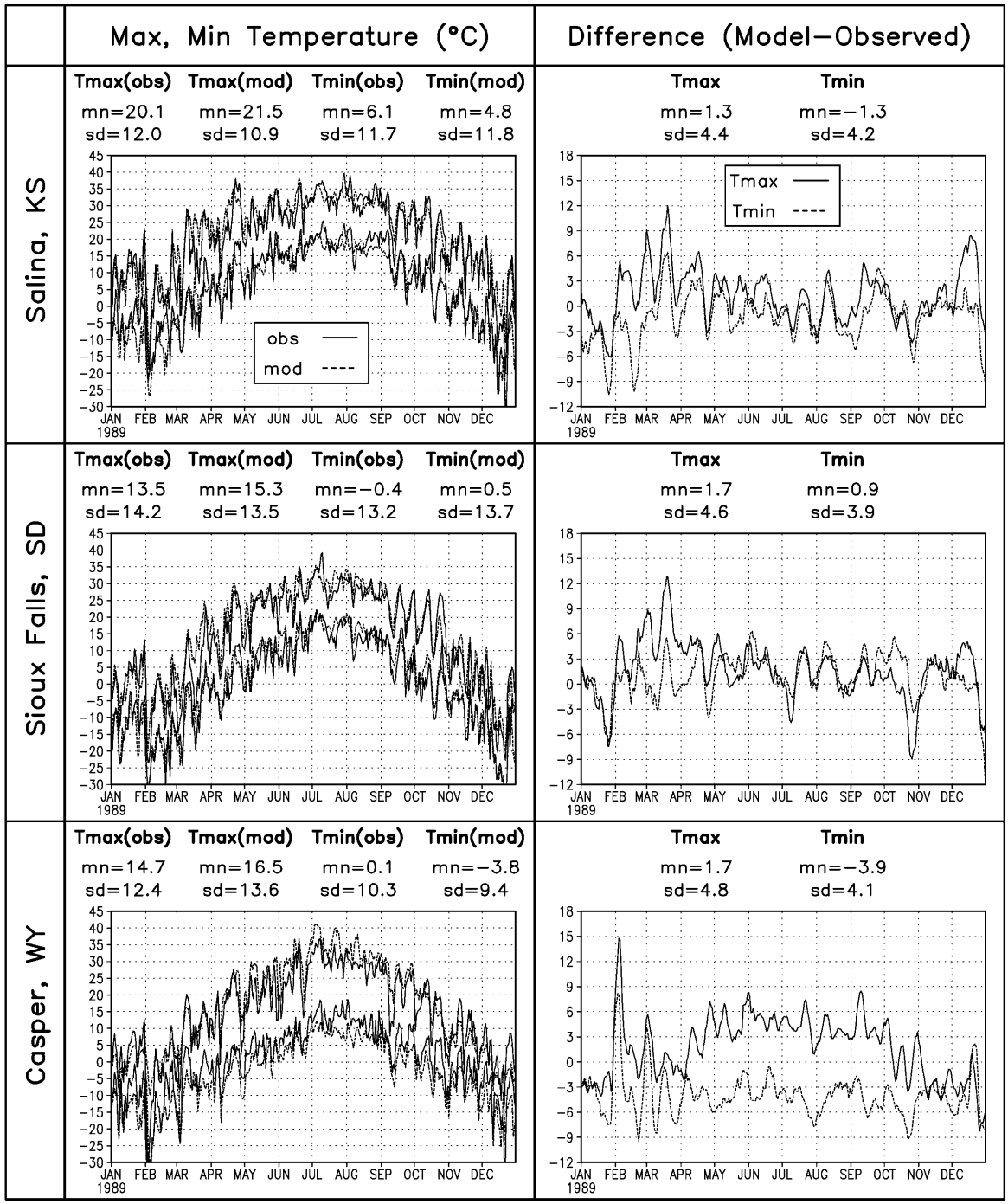

Fig. 11. The annual cycle of daily maximum and minimum screen-height temperature at the model grid cells corresponding to three cities identified by the markers in Fig. 6. Also shown is the difference between the model and observations, plotted using a 7-day running mean to improve clarity. Included are the mean (mn) and standard deviation (sd) for each panel and variable; the statistics for the difference plots were computed using the original data, prior to applying the running mean

on specific days. For the cases of Salina and Sioux Falls, the annual average differences are less than a couple of degrees. Casper has a similar annual average difference for the maximum temperature, but the modeled minimum temperature is 3.9 °C low. In addition, the modeled summer maximum temperatures are consistently high. In the more mountainous regions of the domain we expect it to be more difficult to model the local terrain forcing that

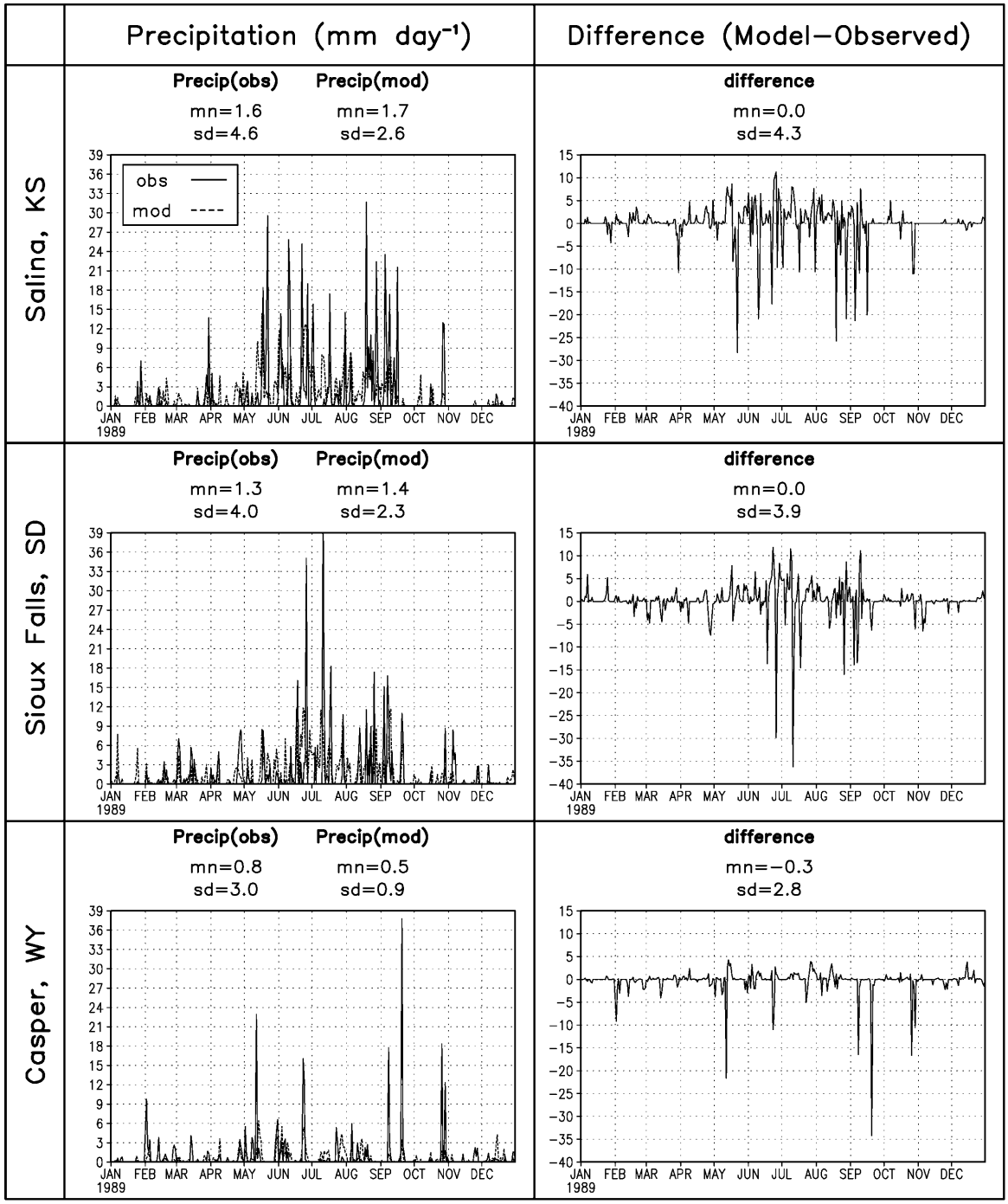

Fig. 12. The annual cycle of daily precipitation at the model grid cells corresponding to three cities identified by the markers in Fig. 6. Also shown is the difference between the model and observations. Included are the mean (mn) and standard deviation (sd) for each panel and variable

strongly influences weather and climate features there. Many of these forcings exist as scales below those resolved by the 50-km grid used in these simulations.

The annual cycle of daily precipitation is provided in Fig. 12, for the same three cities used in Fig. 11 (see Fig. 6). These stations are able to capture some of the regional variation that exists within this domain; Casper receives significantly less precipitation than the prairie cites. Again it is clear that the model does not generally capture the peak magnitudes of the precipitation events,

as shown by the negative tails in the difference plots, but the timing of individual events and the synoptic and seasonal cycles are well simulated.

5. Discussion and conclusions

ClimRAMS, a climate version of the Regional Atmospheric Modeling System (RAMS) has been used to simulate atmospheric and land-surface processes during 1989, over a portion of the Great Plains and Rocky Mountains of the United States. The year 1989 was reasonably close to the climate averages for the region being considered. This regional climate modeling study is unique in that it has used daily observations to validate the model outputs. While the diurnal cycle is not explicitly analyzed with sub-daily observational data, it is implicitly addressed through the use of daily maximum and minimum air-temperature data sets. Application of these daily data, as opposed to monthly-mean data typically used in the past, has allowed demonstration of the model's ability to capture the synoptic cycles that dominate middle-latitude weather and climate characteristics. On even finer temporal scales, the model has been found to generally simulate daily maximum and minimum screen-height air temperatures and daily precipitation. Thus, ClimRAMS has been shown to simulate the daily- to synoptic-scale atmospheric forcing that collectively merges to define the climate of a region. Using six-hourly NCEP reanalysis data to define the atmospheric lateral boundary conditions, at approximately the outer boundaries of the conterminous United States, the model has successfully transferred that information into the interior of the domain, roughly the central United States. The model's analysis domain includes portions of the Great Plains and Rocky Mountains and, as such, within this domain there are both north-south and east-west gradients of important climatological variables such as temperature and precipitation. The model has been able to simulate these spatial distributions, as well as their temporal evolution throughout the year.

Prior to comparing the modeled and observed screen-height air temperatures, the modeled data was corrected to the observation-station elevations by applying a constant lapse rate to the elevation differences between model and stations. In the natural system, the lapse rate varies in both time and space, and is a function of many factors, including atmospheric moisture and stability conditions. Implementing a more sophisticated elevation correction would likely change the details of our results, but is not expected to change any of our general conclusions regarding the model's ability to simulate the observed weather and climate.

In spite of the general success of the model, errors in the simulation of the basic observed climatological fields still suggest that significant model improvements can and should be made. Modeled errors can be the result of several factors that are often interrelated. For example, changes to the precipitation scheme lead to differences in cloudiness that affect shortwave and longwave radiation reaching the ground. This, in turn, modifies surface energy fluxes, temperatures, and soil moisture; all of which influence cloud and precipitation processes. As part of the model development and other studies using ClimRAMS (e.g., Lu et al., 2001), improvements to the model's definition of the seasonal evolution of vegetation parameters, like LAI and albedo, have been suggested. In the future we anticipate being able to use remotely-sensed data sets to help define these quantities and make them more realistic. The soil moisture distribution and evolution is also something that the model simulates, and its values influence surface energy and moisture fluxes, and air temperature and humidity. Unfortunately, there are only limited soil moisture observations, and the exact modeled biases are unclear. We also know that the natural system displays land-surface variability at scales much smaller than that represented by the 50-km grid. To account for this heterogeneity, higher-resolution model simulations are required. In addition, increased vertical resolution is expected to lead to improved representation of the modeled boundary layer. Improvements to any of these model components should improve the model's physical realism, and hopefully the simulated climatologies.

An important attribute of ClimRAMS is its ability to also use the other RAMS components. These include the more complex cloud and precipitation microphysics schemes, and radiation sub-models. For this 50-km grid simulation,

the use of a simple precipitation scheme has been found to provide acceptable results. Identical simulations, but using the RAMS full precipitation-microphysics scheme (not shown), did not appreciably improve the model simulation. For higher-resolution simulations, the more complex precipitation scheme has been found to improve results (e.g., Gaudet and Cotton, 1998). In addition, the model's nonhydrostatic and fully-interactive telescoping-grid capabilities allow ClimRAMS to be applied to a wide variety of problems ranging in horizontal scale from a few hundred kilometers to less than one kilometer.

ClimRAMS has been able to realistically simulate the seasonal, synoptic, and diurnal cycles over an entire year. Generally the model errors become greater as the temporal cycle of interest becomes shorter. For example, a one-day shift in a frontal passage will lead to precipitation falling on the wrong day, and this will show up as an error in the model simulation. But, averaged over that synoptic cycle, the precipitation is generally quite realistic. Analyses of the differences between model results and observations suggests that the temperature and precipitation fields are acceptable representations of the region's spatial and temporal climatologies. The general success of the model simulations presented herein suggest that ClimRAMS can be used in support of vegetation- and snow-related evolution and atmospheric interaction studies. These research efforts require an atmospheric model capable of performing realistic annual integrations that include reasonable representations of diurnal, synoptic, and seasonal cycles.

Acknowledgements

Special thanks is extended to T. Kittel who was instrumental in developing the original ideas and funding for this model development effort. The authors would also like to thank J. Copeland, E. Greene, L. Lu, and R. Walko for their assistance in making this modeling effort a success. The land-cover and topographic data used in the model simulations are distributed by the EROS Data Center Distributed Active Archive Center (EDC DAAC), located at the United States Geological Survey's EROS Data Center in Sioux Falls, South Dakota. This work was supported by NOAA Grant NA67RJ0152, NASA Grants NAG5-4760, NAG8-1511, and NAG5-7560, EPA Grant R824993-01-0, NSF Contract OPP-9614632, and NPS Contracts CA 1268-2-9004 COLR-R92-0204 and CEGR-R92-0193.

References

Arakawa A, Lamb RV (1977) Computational design of the basic dynamical processes of the UCLA general circulation model. Methods in Computational Physics 17: 174–265

Auer AH (1974) The rain versus snow threshold temperatures. Weatherwise 27: 67

Avissar R, Mahrer Y (1982) Verification study of a numerical greenhouse microclimate model. Trans Amer Soc Agric Eng 25: 1711–1720

Beniston M (1998) From turbulence to climate: numerical investigations of the atmosphere with a hierarchy of models. New York: Springer, 328 pp

Businger JA, Wyngaard JC, Izumi Y, Bradley EF (1971) Flux-profile relationship in the atmospheric surface layer. J Atmos Sci 28: 181–189

Carroll TR (1997) Integrated observations and processing of snow cover data in the NWS hydrology program, Proceedings of the 77th AMS Annual Meeting. Symposium on Integrated Observing Systems, Long Beach, California, pp 180–183

Chen C, Cotton WR (1983) A one-dimensional simulation of the stratocumulus-capped mixed layer. Bound-Layer Meteor 25: 289–321

Chen C, Cotton WR (1987) The physics of the marine stratocumulus-capped mixed layer. J Atmos Sci 44: 2951–2977

Clapp R, Hornberger G (1978) Empirical equations for some soil hydraulic properties. Water Resour Res 14: 601–604

Clark TL (1977) A small-scale dynamic model using a terrain-following coordinate transformation. J Comp Phys 24: 186–215

Clark TL, Farley RD (1984) Severe downslope windstorm calculations in two and three spatial dimensions using anelastic interactive grid nesting: A possible mechanism for gustiness. J Atmos Sci 41: 329–350

Clark TL, Hall WD (1991) Multi-domain simulations of the time dependent Navier-Stokes equations: Benchmark error analysis of some nesting procedures. J Comput Phys 92: 456–481

Copeland JH, Pielke RA, Kittel TGF (1996) Potential climatic impacts of vegetation change: A regional modeling study. J Geophys Res 101(D3): 7409–7418

Cotton WR, Weaver JF, Beitler BA (1995) An unusual summertime downslope wind event in Fort Collins, Colorado, on 3 July 1993. Wea and Forecasting 10: 786–797

Cressman GP (1959) An operational objective analysis system. Mon Wea Rev 87: 367–374

Christensen JH, Machenhauer B, Jones RG, Schär C, Ruti PM, Castro M, Visconti G (1997) Validation of present-day regional climate simulations over Europe: LAM simulations with observed boundary conditions. Climate Dynamics 13: 489–506

Christensen OB, Christensen JH, Machenhauer B, Botzet M (1998) Very high-resolution regional climate simulations over Scandinavia – present climate. J Climate 11: 3204–3229

Davies HC (1976) A lateral boundary formulation for multi-level prediction models. Quart J Roy Meteor Soc 102: 405–418

Davies HC (1983) Limitations of some common lateral boundary schemes used in regional NWP models. Mon Wea Rev 111: 1002–1012

Deardorff JW (1978) Efficient prediction of ground surface temperature and moisture, with inclusion of a layer of vegetation. J Geophys Res 83(C4): 1889–1903

Dickinson RE, Henderson-Sellers A, Kennedy PJ, Wilson MF (1986) Biosphere-Atmosphere Transfer Scheme (BATS) for the NCAR Community Climate Model. NCAR Tech Note NCAR/TN-275 + STR, 69 pp

Eastman JL (1999) Analysis of the effects of CO_2 and landscape change using a coupled plant and meteorological model. PhD dissertation, Department of Atmospheric Science, Colorado State University, 148 pp

Gal-Chen T, Somerville RCJ (1975) On the use of coordinate transformation for the solution of the Navier-Stokes equations. J Comput Phys 17: 209–228

Gallo KP, Easterling DR, Peterson TC (1996) The influence of land use/and cover on climatological values of the diurnal temperature range. J Climate 9: 2941–2944

Gaudet B, Cotton WR (1998) Statistical characteristics of a real-time precipitation forecasting model. Wea Forecasting 13: 966–982

Gesch DB, Verdin KL, Greenlee SK (1999) New land surface digital elevation model covers the Earth. EOS Transactions, AGU, 80(6): 69–70

Giorgi F (1995) Perspectives for regional earth system modeling. Global and Planetary Change 10: 23–42

Giorgi F, Bates GT, Nieman SJ (1993) The multiyear surface climatology of a regional atmospheric model over the western United States. J Climate 6: 75–95

Groisman PY, Legates DR (1994) The accuracy of United States precipitation data. Bull Amer Meteor Soc 75(3): 215–227

Harrington JY (1997) The effects of radiative and microphysical processes on simulated warm and transition season Arctic stratus. PhD dissertation, Atmospheric Science Paper No. 637, Department of Atmospheric Science, Colorado State University, 289 pp

Hill GE (1974) Factors controlling the size and spacing of cumulus clouds as revealed by numerical experiments. J Atmos Sci 31: 646–673

Hurley P, Boers R (1996) The effect of cloud cover on surface net radiation: simple formulae for use in mesoscale models. Bound-Layer Meteor 79: 191–199

Kalnay E, Kanamitsu M, Kistler R, Collins W, Deaven D, Derber J, Gandin L, Sara S, White G, Woollen J, Zhu Y, Chelliah M, Ebisuzaki W, Higgins W, Janowiak J, Mo KC, Ropelewski C, Wang J, Leetma A, Renolds R, Jenne R (1995) The NMC/NCAR reanalysis project. Bull Amer Meteor Soc 77: 437–471

Karl TR, Diaz HF, Kukla G (1988) Urbanization: Its detection and effect in the United States climate record. J Climate 1: 1099–1123

Kuo HL (1974) Further studies of the parameterization of the influence of cumulus convection on large-scale flow. J Atmos Sci 31: 1232–1240

Lilly DK (1962) On the numerical simulation of buoyant convection. Tellus 14: 148–172

Liston GE, Pielke Sr RA, Greene EM (1999) Improving first-order snow-related deficiencies in a regional climate model. J Geophys Res 104(D16): 19559–19567

Louis JL (1979) A parametric model of vertical eddy flux in the atmosphere. Bound-Layer Meteor 17: 187–202

Louis JL, Tiedtke M, Geleyn JF (1982) A short history of the PBL parameterization at ECMWF. Proc 1981 Workshop on PBL Parameterization, Shinfield Park, Reading, UK, ECMWF pp 59–71

Lu L, Pielke Sr RA, Liston GE, Parton WJ, Ojima D, Hartman M (2001) Implementation of a two-way interactive atmospheric and ecological model and its application to the Central United States. J Climate 14: 900–919

Lüthi D, Cress A, Davies HC, Frei C, Schär C (1996) Interannual variability and regional climate simulations. Theor Appl Climatol 53: 185–209

Mahrer Y, Pielke RA (1977) A numerical study of the airflow over irregular terrain. Beiträge zur Physik der Atmosphäre 50: 98–113

Male DH, Gray DM (1981) Snowcover ablation and runoff. In: Gray DM, Male DH (eds) Handbook of Snow – Principles, Processes, Management and Use. Toronto: Pergamon Press, pp 360–436

Marinucci MR, Giorgi F, Beniston M, Wild M, Tschuck P, Ohmura A, Bernasconi A (1995) High resolution simulations of January and July climate over the Western Alpine Region with a nested regional climate modeling system. Theor Appl Climatol 51: 119–138

McCumber MC, Pielke RA (1981) Simulation of the effects of surface fluxes of heat and moisture in a mesoscale numerical model, Part I: Soil layer. J Geophys Res 86: 9929–9938

McGregor JL (1997) Regional climate modelling. Meteorol Atmos Phys 63: 105–117

Mearns LO, Giorgi F, McDaniel L, Shields C (1995) Analysis of variability and diurnal range of daily temperature in a nested regional climate model: comparison with observations and doubled CO_2 results. Climate Dynamics 11: 193–209

Meyers MP (1995) The impact of a two-moment cloud model on the microphysical structure of two precipitation events. Ph D dissertation, Atmospheric Science Paper No. 575, Department of Atmospheric Science, Colorado State University, 165 pp

Meyers MP, DeMott PJ, Cotton WR (1992) New primary ice nucleation parameterizations in an explicit cloud model. J Appl Meteor 31: 708–721

Miller DA, White RA (1998) A conterminous United States multi-layer soil characteristics data set for regional climate and hydrology modeling. Earth Interactions 2 (Available on-line at http:// EarthInteractions.org)

Molinari J (1985) A general form of Kuo's cumulus parameterization. Mon Wea Rev 113: 1411–1416

Neiburger M (1949) Reflection, absorption, and transmission of insolation by stratus cloud. J Appl Meteor 6: 98–104.

Nicholls ME, Pielke RA, Eastman JL, Finley CA, Lyons WA, Tremback CJ, Walko RL, Cotton WR (1995) Appli-

cations of the RAMS numerical model to dispersion over urban areas. In: Cermak JE et al (eds) Wind Climate in Cities. The Netherlands: Kluwer Academic Publishers, pp 703–732

Parton WJ, Ojima DS, Schimel DS (1996) Models to evaluate soil organic matter storage and dynamics. In: Carter MR, Stewart BA (eds) Structure and Organic Matter Storage in Agricultural Soils. New York: CRC Press, pp 421–448

Philip JR, DeVries DA (1957) Moisture movement in porous materials under temperature gradients. Trans Amer Geophys Union 38: 222–232

Pielke RA (1974) A three-dimensional numerical model of the sea breezes over south Florida. Mon Wea Rev 102: 115–139

Pielke RA, Cotton WR, Walko RL, Tremback CJ, Lyons WA, Grasso LD, Nicholls ME, Moran MD, Wesley DA, Lee TJ, Copeland JH (1992) A comprehensive meteorological modeling system–RAMS. Meteorol Atmos Phys 49: 69–91

Reynolds RW, Smith TM (1994) Improved global sea surface temperature analyses using optimum interpolation. J Climate 7: 929–948

Rhea JO (1978) Orographic precipitation model for hydrometeorological use. Ph D dissertation, Atmospheric Science Paper No. 287, Department of Atmospheric Science, Colorado State University, 199 pp

Sturm M, Holmgren J, Liston GE (1995) A seasonal snow cover classification system for local to global applications. J Climate 8: 1261–1283

Schultz P (1995) An explicit cloud physics parameterization for operational numerical weather prediction. Mon Wea Rev 123: 3331–3343

Smagorinski J (1963) General circulation experiments with the primitive equations. Part I, The basic experiment. Mon Wea Rev 91: 99–164

Takle ES, Gutowski Jr WJ, Arritt RW, Pan Z, Anderson CJ, de Silva RR, Caya D, Chen S-C, Giorgi F, Christensen JH, Hong S-Y, Juang H-M H, Katzfey J, Lapenta WM, Laprise R, Liston GE, Lopez P, McGregor J, Pielke Sr RA, Roads, JO (1999) Project to Intercompare Regional Climate Simulations (PIRCS): Description and initial results. J Geophys Res 104(D16): 19443–19461

Thompson G (1993) Prototype real-time mesoscale prediction during 1991–92 winter season and statistical verification of model data. MS thesis, Dept of Atmospheric Science, Colorado State University, 105 pp

Tremback CJ (1990) Numerical simulation of a mesoscale convective complex: Model development and numerical results. PhD dissertation, Atmospheric Science Paper No. 465, Department of Atmospheric Science, Colorado State University, 247 pp

Tremback CJ, Kessler R (1985) A surface temperature and moisture parameterization for use in mesoscale numerical models. Preprints, 7th Conference on Numerical Weather Prediction, Montreal, Canada, AMS, 17–20 June, pp 355–358

Tremback CJ, Tripoli GJ, Cotton WR (1985) A regional scale atmospheric numerical model including explicit moist physics and a hydrostatic time-split scheme. Preprints, 7th Conference on Numerical Weather Prediction, Montreal, Quebec, AMS, 17–20 June, pp 433–434

Tripoli GJ, Cotton WR (1980) A numerical investigation of several factors contributing to the observed variable intensity of deep convection over South Florida. J Appl Meteor 19: 1037–1063

Tripoli GJ, Cotton WR (1982) The Colorado State University three-dimensional cloud/mesoscale model–1982, Part I: General theoretical framework and sensitivity experiments. J de Rech Atmos 16: 185–220

Walko RL, Cotton WR, Meyers MP, Harrington JH (1995a) New RAMS cloud microphysics parameterization, Part I: the single-moment scheme. Atmos Res 38: 29–62.

Walko RL, Tremback CJ, Pielke RA, Cotton WR (1995b) An interactive nesting algorithm for stretched grids and variable nesting ratios. J Appl Meteor 34: 994–999

Authors' address: Glen E. Liston (liston@iceberg.atmos.colostate.edu) and Roger A. Pielke, Sr., Department of Atmospheric Science, Colorado State University, Fort Collins, CO 80523-1371, USA.